

# DESIGN OF A NON-PERIODIC ARTIFICIAL MAGNETIC CONDUCTOR TO OBTAIN A HIGH-GAIN WIDEBAND LOW-PROFILE ANTENNA

Rosa M. Mateos<sup>(1)</sup>, Christophe Craeye<sup>(1)</sup>, and Giovanni Toso<sup>(2)</sup>

<sup>(1)</sup>*Université catholique de Louvain, Laboratoire TELE, Place du Levant 2, 1348 Louvain-la-Neuve, Belgium, mateos@tele.ucl.ac.be, craeye@tele.ucl.ac.be*

<sup>(2)</sup>*Antenna and sub-millimeter wave section, ESA/ESTEC, 2200 AG Noordwijk, The Netherlands, Giovanni.Toso@esa.int*

## ABSTRACT

The narrow bandwidth of artificial magnetic conductors (AMC's) limits their use in broadband applications. Besides this, when trying to increase the bandwidth of antennas based on high-impedance surfaces, the radiation pattern tends to split at broadside when approaching the resonance frequency of the AMC used as a ground plane. A study on the surface currents on the patches evidences that the currents induced on contiguous patches are not in phase, which may lead to the cancelation of their E-field contributions. In this paper, the dependence of this phase shift versus frequency and patches dimensions is analyzed with the help of an eigenmode analysis based on the Method-of-Moment (MoM) technique. Reducing the size of the AMC in the E-plane and breaking its periodicity in the H-plane improves the broadside directivity.

## 1. INTRODUCTION

Artificial magnetic conductors (AMC's) potentially allow horizontal antennas to be placed very close to the ground-plane surface without being short-circuited by their image. The design of new AMC structures is being studied in many different groups [1]-[3]. However, because of their narrow bandwidth, their application is still a challenge for broadband antennas. Moreover, we have observed that the patterns of an antenna placed above an AMC tend to split at broadside at frequencies near and beyond the AMC resonance [4]. So, the direction of the maximum is no longer at broadside, reducing the real useful band.

Werner optimizes both the antenna and AMC surface simultaneously to achieve improved antenna performances compared with the antenna and the AMC surface optimized separately. Reference [5] presents a broadband prototype operating from 5.5 to 7.1 GHz (25,4% bandwidth) with a gain larger than 7.5 dB over the useful band and a  $0.095\lambda$  profile, where  $\lambda$  is the wavelength at the highest frequency. We tried to provide a further knowledge about what is happening from a more physical point of view. To this end, a study on the currents on

the patches of the AMC structure has been carried out. Phase shifts between successive cells are observed in the  $y$ -component of the surface currents along  $\hat{x}$  and  $\hat{y}$  coordinates [4]. It results in a destructive combination of their broadside E-field contributions at certain frequencies. In the hypothesis of leaky mode radiation ( $k_{LW} = \beta - j\alpha$ , with  $\beta$  and  $\alpha$  standing for the phase and the attenuation constants), the induced currents are homogeneous in phase. Broadside radiation from a leaky-wave antenna (LWA) can be obtained for small but nonzero values of  $\beta$  [6], that is, small phase shifts between contiguous elements of the AMC. Thus, in this paper, a further analysis on the dependence of the surface currents phase shifts versus frequency and AMC patches length is carried out with the help of a home-made code based on the MoM numerical technique.

A rectangular  $6 \times 2$  non-periodic AMC has been proposed as a solution to overcome the splitting patterns problem observed at broadside when using a dual-dipole antenna as radiating element [4]. The central patches just below the antenna play the role of AMC, while the patches of different sizes along the antenna act as a guiding surface with an homogeneous phase between adjacent elements. By appropriately adjusting the dimensions of the new prototype, a design providing more than 9.2 dB over a 32.6% bandwidth has been achieved [4]. The antenna profile in such a case is equal to  $0.15\lambda$ , where  $\lambda$  corresponds to the wavelength at the highest frequency. This task has been performed with the help of the FEKO [7] software, a full-wave simulation tool also based on the Method of Moments (MoM).

This paper is organized as follows. Section 2 presents the splitting patterns problem, together with the new AMC design proposed as a solution. It also contains the study on the surface currents on the patches of the AMC structure, in order to have better insight on what is happening at the frequencies where the broadside directivity is bad. Section 3 briefly reviews the theory for the periodic Green's function developed with MoM technique, to set the basis of the eigenmode analysis provided in Section 4. Conclusions are drawn in Section 5.

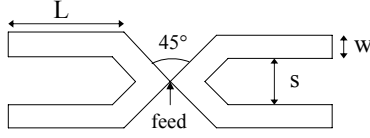


Figure 1. Design parameters ( $w$ ,  $L$  and  $s$ ) of the antenna studied.

## 2. HIGH-GAIN WIDEBAND LOW-PROFILE ANTENNA

### 2.1. Patterns splitting at broadside

A double planar dipole antenna located above an AMC is studied in [4]. Fig. 2 shows the double-dipole antenna horizontally placed above the AMC surface. It is fed at a central common point by means of a voltage gap. The dipoles width  $w$  and length  $L$ , along with the distance  $s$  between them are the design parameters (Fig. 1). The AMC consists of an array of metallic patches separated by a 0.5 mm gap and placed 1 mm above a metal sheet. Air (or foam) fills the space between the patches and the ground plane. Initially, a periodic array of  $6 \times 6$  square patches of 3 mm length plays the role of AMC. It is observed that impedance bandwidths ( $S_{11} < -10$  dB) around 30% can be achieved if the dipole antenna is tuned to work close to the AMC resonance. In contrast, the broadside directivity decreases around the AMC resonance, reaching deep negative values (in dB) at frequencies beyond it (dashed line in Fig. 3).

### 2.2. Rectangular non-periodic AMC

In order to overcome this problem, the AMC size has been reduced in the H-plane of the antenna and made non-periodic in the E-plane (see Fig. 2). The resulting AMC structure is a rectangular surface of  $6 \times 2$  patches of different sizes. The patch length gradually decreases from the center of the structure along the  $\hat{y}$  coordinate, and it does not change along  $\hat{x}$ . The size  $L_c$  of the central square patches is chosen to tune the AMC resonance frequency, while the length difference between contiguous patches  $L_{dec}$  is taken constant. Using the new AMC structure as a ground plane strongly improves the directivity achieved at broadside near and beyond the AMC resonance (solid line in Fig. 3), and does not especially affect the impedance bandwidth performances [4]. Reference [4] also shows that for bigger differences between patches, slightly higher directivity values are obtained.

Once the patterns splitting problem is solved, a high-gain wideband low-profile antenna can be achieved by tuning the dipole antenna and AMC parameters. A design providing more than 9.2 dB over a 32.6% bandwidth with a  $\lambda_{min}/6.5$  profile is presented in [4]. The horizontal dimensions of the structure are  $1.9\lambda_{min} \times 0.7\lambda_{min}$ .

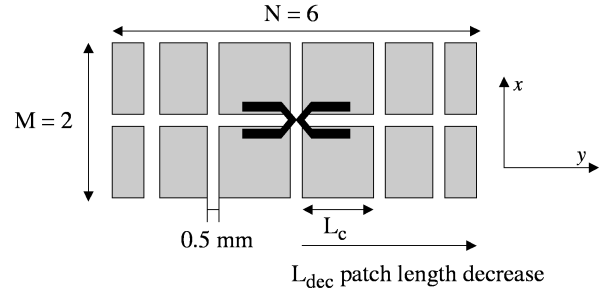


Figure 2. Dimensions of the non-periodic  $6 \times 2$  PMC with the dual-dipole antenna above.

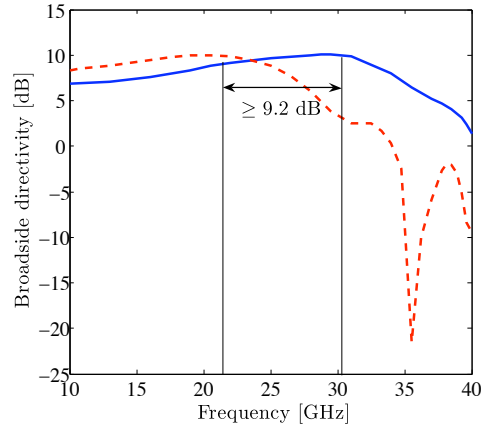


Figure 3. Broadside directivity for initial (dashed) and final (solid) designs.

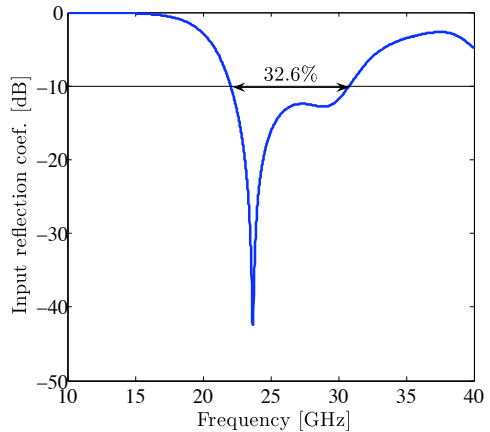


Figure 4.  $S_{11}$  coef. w.r.t.  $50 \Omega$  for the final design.

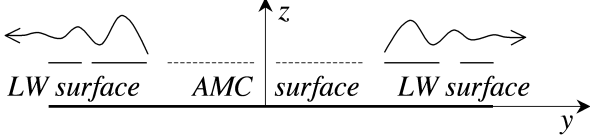


Figure 5. Combination of the leaky mode and AMC phenomena in the same structure.

### 2.3. Currents on patches

A study of the currents on the patches of the AMC provides us a better understanding of what is happening at the frequencies where the patterns split. A frequency equal to 35.5 GHz, for which deep negative directivity values are observed (Fig. 3), has been chosen. The dual-dipole antenna is linearly-polarised along the  $\hat{y}$  coordinate. When looking at the phase of the  $\hat{y}$  component of the surface currents ( $J_y$ ) induced on the patches along the  $\hat{x}$  coordinate, a phase shift close to 180 degrees is observed when considering a  $6 \times 6$  periodic AMC surface. Such a shift yields a cancelation of the contribution of each patch to the radiated E-field. When reducing the number of patches perpendicularly to the antenna (a  $6 \times 2$  prototype appears), we avoid such destructive effect and the radiation at broadside is improved [4]. If we do the same analysis for successive patches in the  $\hat{y}$  coordinate, we observe that breaking the periodicity of the  $6 \times 2$  AMC in this direction reduces the  $J_y$  phase shift between contiguous patches [4]. It is also seen that bigger differences of the patch length ( $L_{dec}$ ) result in smaller currents phase shifts. Such phenomena supports the directivity improvements evidenced in Fig. 3.

If a guiding effect is achieved, the surface will be illuminated in a uniform way. If in addition we obtain an illumination with an homogeneous phase along successive elements, leaky waves will propagate and radiate. We want to study the effect of such phenomenon combined with AMC surfaces (see Fig. 5). With an eigenmode analysis we want to have a better insight on the relation between the phase of the induced currents on the patches of the AMC and some of the surface parameters.

## 3. MOM FORMULATION

The geometry of the array of grounded square patches under consideration is shown in Fig. 6. It is an infinite array in  $x$  and  $y$  directions with interelement spacings denoted by  $d_x$  and  $d_y$ , respectively.  $L_p$  stands for the patches length.

### 3.1. Periodic Green's function

The Green's function for the scalar potential related to an array infinite along  $\hat{x}$  and  $\hat{y}$  can be written as

$$A(\vec{r}) = \sum_{n=-\infty}^{\infty} \sum_{m=-\infty}^{\infty} \frac{e^{-jkR_{mn}}}{4\pi R_{mn}} e^{-jm\psi_x} e^{-jn\psi_y} \quad (1)$$

where  $k$  is the free space wave number,  $R_{mn}$  is the distance between the observation point  $\vec{r} = (x, y, z)$  and the  $m$ th source point  $\vec{r}' = (md_x, nd_y, 0)$ , and  $\psi_x, \psi_y$  stand for the phase shift between adjacent elements in the  $x$  and  $y$  directions, respectively.

$$\psi_x = kd_x \sin \theta \cos \phi + 2\pi m \quad (2)$$

$$\psi_y = kd_y \sin \theta \sin \phi + 2\pi n \quad (3)$$

The pair  $(\theta, \phi)$  represents the incidence angles.

As done in [8], the infinite periodic Green's function can be expressed via the zeroth-order Hankel function of second kind  $H_0^{(2)}$ ,

$$A(\vec{r}) = \frac{1}{4jd_y} \sum_{m=-\infty}^{\infty} e^{-jm\psi_x} \sum_{n=-\infty}^{\infty} e^{-jk_n y} H_0^{(2)}(\gamma_n R_m) \quad (4)$$

where  $R_m = \sqrt{(x - md_x)^2 + z^2}$  corresponds to the distance to successive source points along  $x$  and

$$\gamma_n^2 = k^2 - k_n^2 = k^2 - \left( \frac{\psi_y}{d_y} + n \frac{2\pi}{d_y} \right)^2 \quad (5)$$

For indexes  $n$  leading to real values of  $\gamma_n$  ( $\gamma_n^2 > 0$ ), we obtain propagating cylindrical waves described by the Hankel functions  $H_0^{(2)}$ . It is interesting to observe that the number of these waves corresponds to the number of main and grating lobes that appear in the visible region. For an imaginary value of  $\gamma_n$  ( $\gamma_n^2 < 0$ ), the Hankel function becomes a rapidly decaying modified Bessel function of the first kind (Eq. 6), which represents evanescent cylindrical waves.

$$H_0^{(2)}(\gamma_n R_m) = H_0^{(2)}(-j\alpha R_m) = \frac{2j}{\pi} K_0(\alpha R_m) \quad (6)$$

with attenuation coefficient  $\alpha = \sqrt{-\gamma_n^2}$  real and positive. The evaluation of the Hankel functions involved in the Green's function  $A$  is relatively time consuming. Thus, the Green's function is tabulated in a 2-D ( $y, R_m$ ) table, which reduces the computation time.

### 3.2. System of equations

The currents induced on the patches of the infinite array are decomposed into a set of  $N$  basis functions  $\vec{J}_i$

$$\vec{J} = \sum_{i=1}^N x_i \vec{J}_i \quad (7)$$

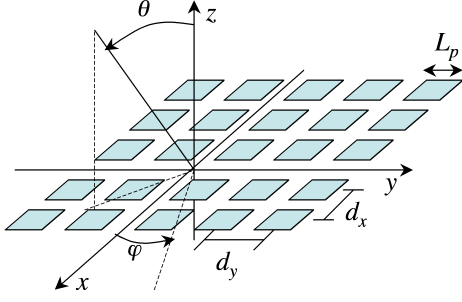


Figure 6. Geometry of the infinite array of grounded patches under study.

where  $x_i$  are the unknown coefficients to be determined. When the surface is excited, the MoM system of equations reads:

$$Zx = v \quad (8)$$

where  $Z$  is the MoM impedance matrix, and the  $t$ th element of the excitation vector  $v$  is obtained as the convolution of the impressed electric field  $\vec{E}^i$  with the testing function  $\vec{J}_t$

$$v_t = - \iint_S \vec{E}^i \vec{J}_t dS \quad (9)$$

If we look for the resonances of the structure, all elements of  $v$  are zero (no excitation) and the resolution of the equations system Eq. 8 becomes an eigenvalues problem. The matrix impedance  $Z$  depends, in our case, on  $\psi_x$  and  $\psi_y$ , it is  $Z(\psi_x, \psi_y)$ . The values of  $\psi_x$  and  $\psi_y$  that make the determinant of  $Z$  equal to zero correspond to the eigenmodes of the structure.

#### 4. EIGENMODES ANALYSIS

We want to analyse the dependence of these phase shifts on the patch dimensions of an infinite periodic AMC and versus frequency. To this end, an eigenmode analysis of the MoM impedance matrix  $Z(\psi_x, \psi_y)$  has been carried out. The determinant of  $Z(\psi_x, \psi_y)$  is evaluated for different values of  $\psi_x$  and  $\psi_y$ . We are specially interested in the behavior of  $\psi_y$ , so  $\psi_x$  is fixed to zero. The  $\psi_y$  testing range has been limited from zero (because of symmetry reasons) to the visible range  $kd_y$  (to avoid grating lobes). Thus, the highest the frequency or the biggest the cell dimensions, the largest  $\psi_y$  testing range. Such analysis has been firstly done at different frequencies for an infinite AMC with patches of length equal to 3 mm. The determinant of  $Z(0, \psi_y)$  normalized w.r.t. its maximum value is plotted in Fig. 7 for three different frequencies. It is interesting to notice that the phase shift  $\psi_y$  between adjacent patches corresponding to an eigenvalue solution ( $|Z(0, \psi_y)| = 0$ ) is bigger at the frequencies where the patterns split: 27.4 GHz (AMC resonance) and 35.5 GHz. At the frequency of 20 GHz (no broadside splitting appears), the lowest determinant of  $Z(0, \psi_y)$  occurs for  $\psi_y$  equal to zero.

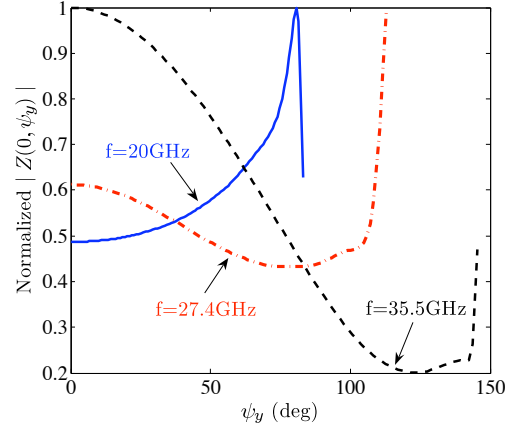


Figure 7. Determinant of the  $Z(0, \psi_y)$  matrix obtained at different frequencies for an infinite AMC with patches of side equal to 3 mm.

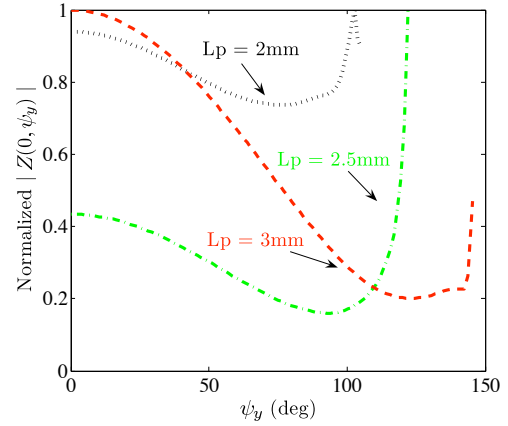


Figure 8. Determinant of the  $Z(0, \psi_y)$  matrix obtained at  $f=35.5$  GHz for infinite AMC surfaces with patches of different size.

The same analysis has been carried out at a fixed frequency (35.5 GHz) for an AMC with patches of different lengths. Fig. 8 shows that reducing the size of the patches decreases the phase shift obtained at the resonances of the AMC structure. Small phase shifts between adjacent elements is a necessary condition for high gain. It is also worth noticing that the determinant curve is flatter for smaller patches.

#### 5. CONCLUSION

Artificial magnetic conductors (AMC) allow to reduce the profile of antennas grounded by such surfaces. However, the radiation patterns split near and beyond the resonance frequency of the AMC, limiting their useful bandwidth. The currents induced on successive patches of the AMC below a dipole-type antenna are not in phase, producing a the cancelation of their E-field contributions

and a dip in the pattern at broadside. An eigenmode analysis based on an infinite-array approach shows that smaller patch sizes reduces the phase shift between adjacent patches; small phase shifts form a necessary condition to achieve a high gain. A  $6 \times 2$  AMC with decreasing patch length along the antenna is designed and proposed to overcome the splitting patterns problem. The central patches allow us to take advantage of the AMC properties to create a low-profile design, and the patches of different sizes help to make more uniform the phase of the currents induced on them, acting as guiding structure. Further work will focus on a more systematic analysis of leaky mode phenomena and on their combined operation with AMC surfaces. A design providing a gain larger than 9.2 dB over a 32.65 % bandwidth is presented. The final dimensions are  $1.9\lambda_{min} \times 0.7\lambda_{min}$  with a  $\lambda_{min}/6.5$  profile.

## ACKNOWLEDGEMENT

This work has been supported by ESA/ESTEC, contract n° 17576/03/NL/LvH.

## REFERENCES

- [1] Yang F. and Rahmat-Samii Y., "Reflection Phase Characterizations of the EBG Ground Plane for Low Profile Wire Antenna Application", *IEEE Trans. Anten. and Propag.*, Vol. 51, 2691-2702, October 2003.
- [2] Sievenpiper D., Zhang L., Broas R., Alexopolous N.G. and Yablonovitch E., "High-impedance electromagnetic surfaces with a forbidden frequency band", *IEEE Trans. Microwave Theory and Techniques*, Vol. 47, 2059-2074, November 1999.
- [3] Zhang Y., J. von Hagen, Younis M., Fischer C. and Wiesbeck W., "Planar artificial magnetic conductors and patch antennas", *IEEE Trans. Antennas and Propagation*, Vol. 51, 2704-2712, October 2003.
- [4] Mateos R.M., Craeye C. and Toso G., "High-gain wideband low-profile antenna", accepted for publication in *Microwave Opt. Techn. Let.*, April 2006.
- [5] Kern D.J., Spence T.G. and Werner D.H., "The Design Optimization of Antennas in the Presence of EBG AMC Ground Planes", *IEEE AP-S International Symposium and USNC/URSI National Radio Science Meeting*, Washington DC, July 2005.
- [6] Lovat G., Burghignoli P. and Jackson D.R., "Fundamental Properties and Optimization of Broadside Radiation From Uniform Leaky-Wave Antennas", *IEEE Trans. Antennas and Propagation*, Vol. 54, 1442-1452, May 2006.
- [7] <http://www.feko.co.za>
- [8] Craeye C. and Dardenne X., "Element Pattern Analysis of Wide-Band Arrays With the Help of a Finite-by-Infinite Array Approach", *IEEE Trans. Antennas and Propagation*, Vol. 54, 519-526, February 2006.